Supplementary Information for "Pressure fluctuations of liquids under short-time acceleration" written by Kurihara, Kiyama and Tagawa.

1 Pressure Measurement by a Hydrophone

As we discuss the pressure wave propagation, we attempted to measure the pressure in liquid directly, by using a needle-type hydrophone. Here, we report the pressure data from a systematic experiment, in which we see a qualitative agreement with our model. We note that this measurement leaves a clear limitation, which should be taken as a caveat for further discussion.

1.1 General Behavior

We show the pressure data measured by using a hydrophone (see figure SI-1 for the setup) for various drop heights H in figure SI-2. The working fluid is the Milli-Q grade water, which is degassed to reduce the chance of cavitation onset. The hydrophone is calibrated. We varied the drop height H from 1 mm to 25 mm so that we could test if the pressure value was consistent with our model. Overall, the pressure waveform (figure SI-2) was qualitatively consistent with that reported by Yukisada *et al.* (2018). For relatively lower drop heights (black and blue), we observe periodic oscillation for a long time, implying the multiple reflections of pressure waves inside the system. For a higher drop height (red), the first peak was detected but the following pressure form is significantly different from lower cases, possibly hinting at the cavitation onset. The magnitude of the first peak also increased as the drop height H increased.

1.2 Frequency of pressure data

We compare the frequency response of acceleration (red, Case I-A) and the pressure (blue, Case I-B) (see figure SI-3 and table SI-1) data. The accelerometer was mounted on the top of the tube while being glued as reported in the main text. The pressure sensor (Mueller-Platte Needle-type hydrophone) was inserted from the top of the tube as illustrated in figure SI-1. Note that, the impact condition might not be exactly the same as the hydrophone sensors are connected to the data acquisition device via a stiff cable. Furthermore, to minimize the risk of cavitation, we restrict the tube fall height as low as possible. Experimental conditions are summarized in the table SI-1. We observed peak frequencies of 4.31 kHz for acceleration and 4.58 kHz for pressure measurement. This is quantitatively consistent with the theoretical estimate for the propagation of a linear sound wave ($f \sim (c/4L) \approx 1483/(4\times 94\times 10^{-3}) \sim$ 3.94 kHz), while there are differences of 10-20% that has been observed consistently when compared to the simplified theory (Kiyama *et al.*, 2016). It might support our assumption that our acceleration measurement captures the pressure change.

1.3 Magnitude of pressure peak and caveat

For further discussion, we compare the pressures the one actually measured versus the one estimated from the model in the main text, which is essentially the water hammer pressure multiplied by the correction factor. The vertical axis of figure SI-4(a) represents the measured pressure, while the estimated value on the horizontal axis varies as a function of the tube drop height, H. The correction factor is sensitive to the pressure sensor position (see below) and the shape of the pressure wavefront (discussed in the main text). The sensor probe was set at $L_p = 70$ mm above the container bottom. The wavefront is assumed to be

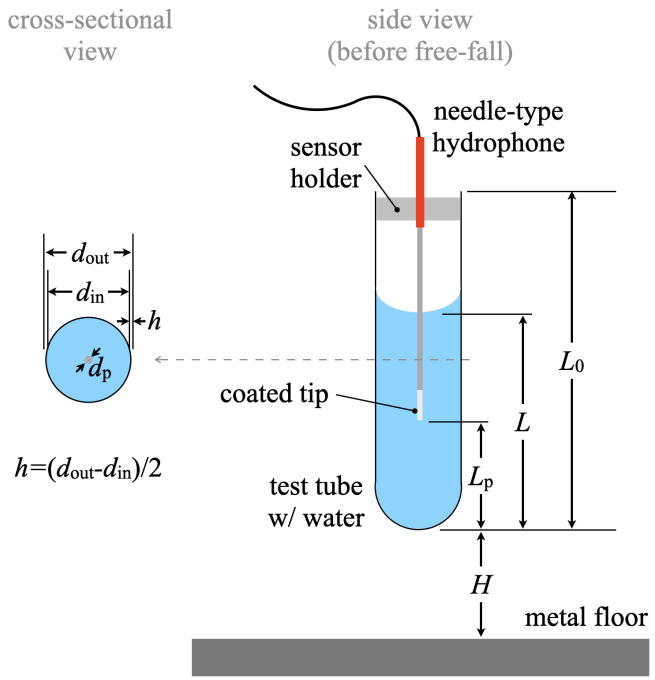

Figure SI-1: Schematic of the setup for the pressure measurement. A needle-type hydrophone is inserted into the liquid-filled test tube, where the sensor is mounted through a holder. L_0, L, L_p and H respectively denote the total tube length, liquid length, the location of a hydrophone tip, and the fall height of the entire system including a tube. A cross-sectional view shows the definitions of inner and outer diameters (d_{in} and d_{out}) and the tube thickness h. d_p represents the diameter of the sensor tip, which might obstacle the pressure wave propagation.

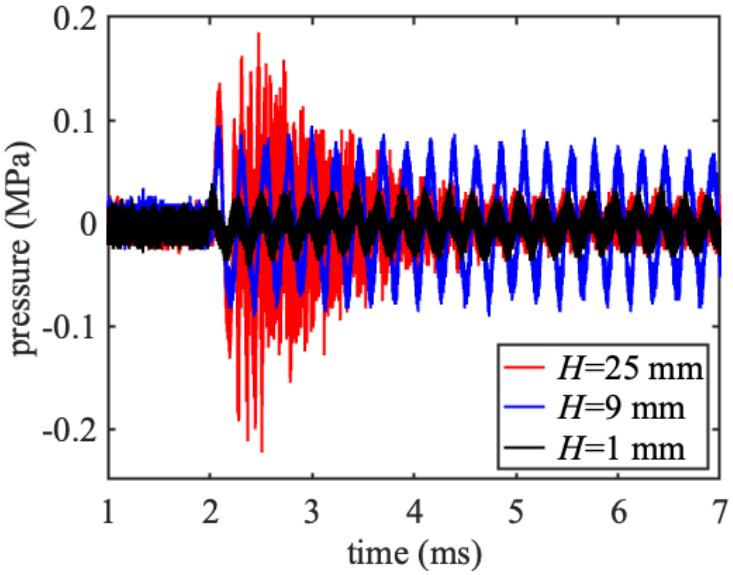

Figure SI-2: Pressure waveform measured by hydrophones. Colors distinguish the tube drop height.

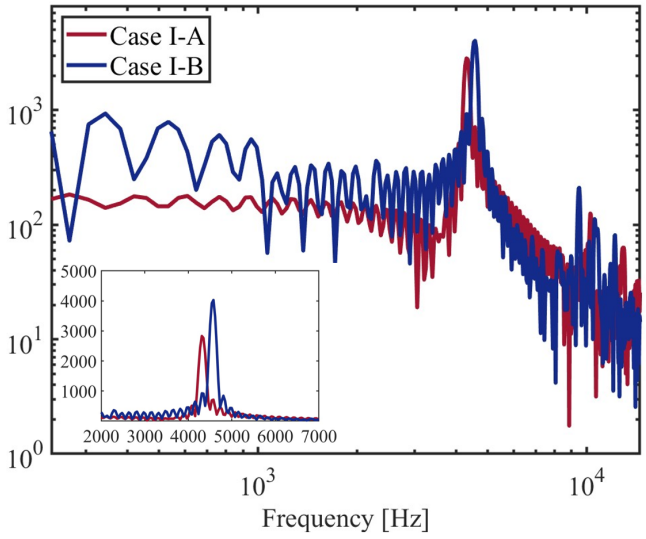

Figure SI-3: Comparison of the dominant frequency of acceleration (red, Case I-A) and pressure (blue, Case I-B) data under similar conditions, presented on a log-log scale. The peak frequencies are 4.31 kHz for the acceleration measurement and 4.58 kHz for the pressure measurement. The inset displays the data on a linear scale.

Table SI-1: Comparison between acceleration and pressure measurements. Here, L_0 represents the height of the test tube, d_{out} and d_{in} denote the outer and inner diameters of the test tube, respectively, h indicates the thickness of the test tube, β quantifies the degree of fluid-structure interaction (see the main text), and L is the liquid height filled in the test tube.

Case	L_0 (mm)	d_{out} (mm)	d_{in} (mm)	h (mm)	β (-)	L (mm)	Measurement type
I-A	105	16.5	14.3	1.1	0.48	94	Accelerometer
I-B	105	16.5	14.3	1.1	0.48	94	Hydrophone

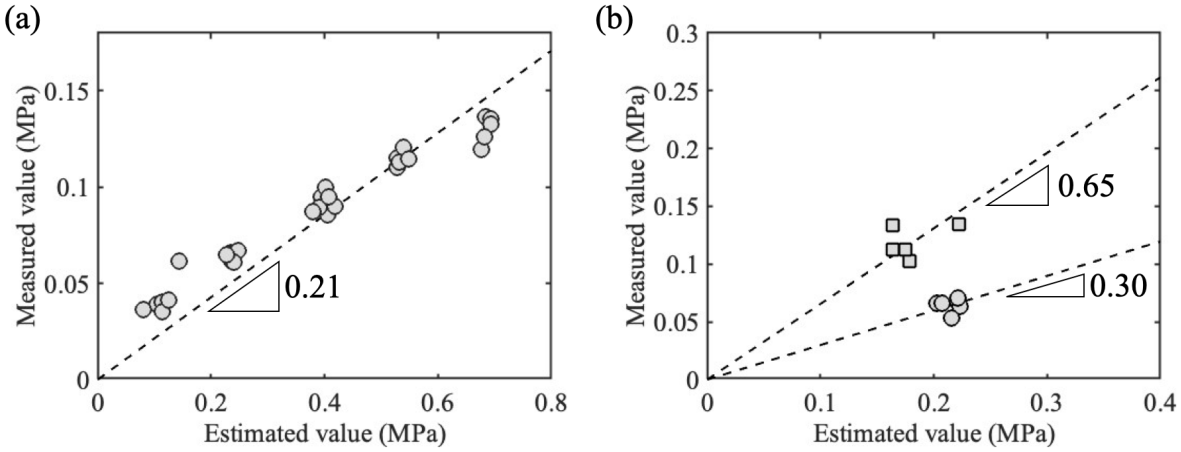

Figure SI-4: (a) Pressure peak value estimated by using a needle hydrophone for various drop heights (1 mm$\leq H \leq$25 mm). (b) Comparison of the pressure output at the same height but using different hydrophones. Marker shapes differentiate between newer (squares) and older (circles) ones.

linear in shape. As can be found in figure SI-4(a), the measured pressure shows a monotonic increment as the tube drop height increases. This indicates that the pressure inside the liquid is controlled by the tube impact velocity, which is the key feature of the water hammer-type model.

We note that the slope remained small (0.21), which means the data might not capture the pressure as expected to be. There are numerous factors possibly involved, including the vibration/relative motion of the hydrophone itself. Here we discuss one of the main contributors. The hydrophone is quite a sensitive sensor. Once the silver coating on its tip (illustrated in figure SI-1) is eroded or peeled off, the sensitivity cannot be trustworthy anymore. This can easily occur when the sensor tip is exposed to impulsive pressure change such as cavitation activity. We repeated the same experiment by using two different hydrophones (figure SI-4(b)). Circles show the data with the one we used for figure SI-4(a), while squares show the data taken by the newest hydrophone we possess. Both hydrophones are calibrated by the manufacturer. The distance from the probe to the tube bottom is set to $L_p = 55$ mm for figure SI-4(b). The tube drop height H was about 1 mm. First of all, a newer hydrophone recorded almost twice the larger value when compared to an older one in a similar experimental condition. This indicates that the quantitative accuracy in the magnitude heavily relies on the choice of sensor, while the frequency responses are still consistent for both sensors. They are indeed reasons why we believe our acceleration-based pressure measurement has an advantage and is needed. The accelerometer can be mounted on the top of the tube without disturbing the flow and pressure field in the system, and thus the influence of the relative motions of the sensor can be minimized. Of course, the sensitivity issue cannot be avoided. However, accelerometers are designed to measure the impulse, which ensures a reasonable robustness.

We would like to note that the pressure measurement also reveals the significant contribution of the shape of the pressure wavefront. In the discussion, we assumed the wavefront to be linear, in which we found a prefactor of 0.65 (figure SI-4(b)). We repeated the experiments while changing the depth of the hydrophone probe to $L_p \approx 75$ mm, where we found a better agreement with the measurement and the model (prefactor: 0.86). This indicates that the shape of the wavefront is much more complex than we initially discussed, which will be the limitation of this work. However, at the same time, we believe this could be a strong reason for considering the influence of the wavefront, supporting the motivation of our work.

2 Influence of the tube deformation/vibration

In the main text, we assumed that the test tube is stiff enough through the estimation of β parameter, which was smaller than the unity. In addition, for the acceleration measurements, the top of the tube was sealed by the accelerometer mount, which is also supposed to reduce the tube vibration/deformation.

We also performed additional experiments while varying thickness of the test tube. For the cases II-B, II-C, and II-D (see table SI-2), we have varied the thickness of the tube h for almost 1.5 times. The primary peak in the acceleration data remains largely the same (see figure SI-5). The theoretical estimate predicts a peak frequency of 4.12 kHz, which is still smaller than the experimental values but remains in the same order of magnitude. We also tested a shallower liquid depth (Cases III-A and -B) and observed qualitatively same trend. From these experiments (figures SI-3 & SI-5), we believe we can reasonably assume the tube is stiff enough, while the range of β values were rather limited.

From the above, it can be hypothesized that the vibration of the interface seen in figure 2 is not caused by the vibration of the tube. To support this further, we conducted additional experiments with various heights of water. Terwagne & Bush (2011) showed a scaling for the frequency of the tube wall when the

Table SI-2: Summary of experimental conditions. Here, L_0 represents the height of the test tube, d_{out} and d_{in} denote the outer and inner diameters of the test tube, respectively, h indicates the thickness of the test tube, β quantifies the degree of fluid-structure interaction (see the main text), and L is the liquid height filled in the test tube.

Case	L_0 (mm)	d_{out} (mm)	d_{in} (mm)	h (mm)	β (-)	L (mm)	Measurement type
II-A	300	16.2	11.9	2.2	0.22	90	Accelerometer
II-B	165	18.0	13.8	2.1	0.26	90	Accelerometer
II-C	165	20.0	14.6	2.7	0.22	90	Accelerometer
II-D	165	22.0	15.6	3.2	0.20	90	Accelerometer
III-A	300	16.2	11.9	2.2	0.22	60	Accelerometer
III-B	165	18.0	13.8	2.1	0.26	60	Accelerometer

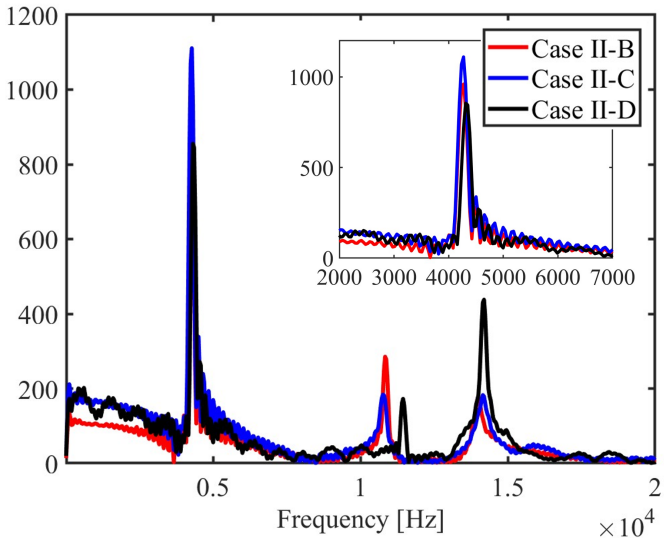

Figure SI-5: Comparison of frequency responses in the acceleration measurement for different thicknesses (i.e., Cases II-B (2.2 mm), II-C (2.7 mm), and II-D (3.2 mm)). The primary peak was found at 4.27 kHz - 4.31 kHz (see also the inset), insensitive to the tube types. As the working fluid was the pure water, estimated dominant frequency of water column in the vertical direction is supposed to be $f_{\text{water}} \approx c/(4L) = 4.12$ kHz, which fairly agrees with the data.

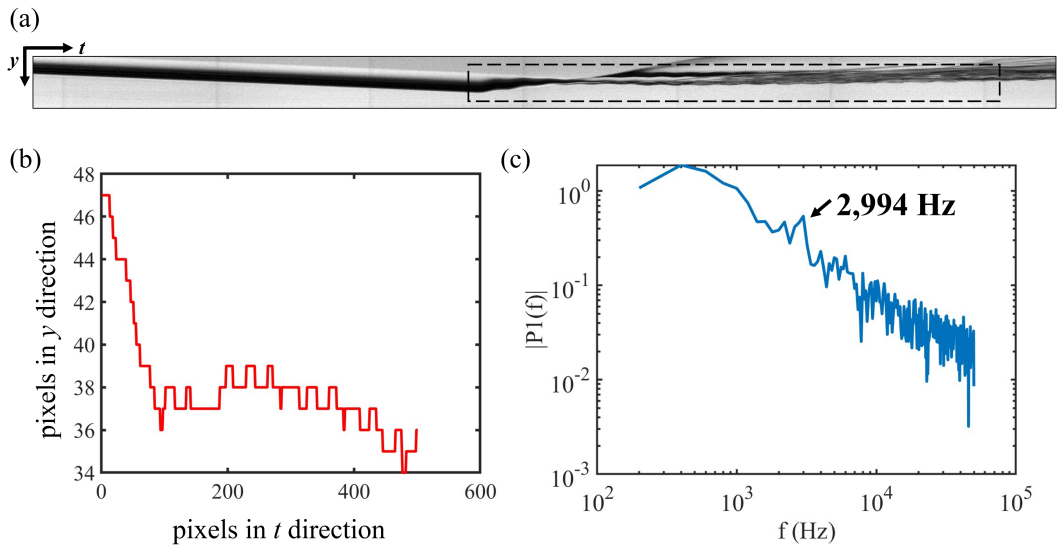

Figure SI-6: (a) A sliced view of the high-speed video, where we focus on the center of the free surface. As shown, the free surface (black area) falls under gravity until it starts vibrating after the impact (marked by a dashed box). (b) Digitized plot for the detected edge (free surface). The FFT result of (b), where we found 2994 Hz for a peak. Here, the silicone oil was used as a working fluid, where the theory estimates the peak frequency of 2685 Hz.

container is partially filled.

$$\frac{f_0}{f_H} \sim \sqrt{1+\frac{\alpha}{5}\frac{\rho_l R}{\rho_s a}\left(\frac{L}{L_0}\right)^4}, \tag{1}$$

where f_0, f_H, α, ρ_l, R, ρ_s, a, L, and L_0 are respectively the tube vibration frequency without liquid, that with liquid, constant (1.25 in their paper), liquid density, tube radius, glass density, thickness of the tube, depth of the liquid and total length of the tube. We have tested two different levels of L/L_0 (see table SI-2, II-A and III-A). Even if we change the liquid heights from 90 mm to 60 mm, equation 1 predicts the ratio of f_H for both heights remains similar to the unity (1.001). On the other hand, the frequency ratio we obtained through experimental measurement was about 1.423, which fairly agreed with the wave propagation scaling (i.e., 90 mm/60 mm=1.5). It might also support our hypothesis that the radial tube vibrations of the container play a somewhat trivial role.

It is noteworthy that the vibration frequency of the free surface indeed agrees with that of the pressure fluctuation. We performed additional analysis for one of the extreme cases where the surface vibration is visible. In this case, silicone oil is filled up to $L \approx$90 mm high. Based on the simple estimation, one obtains the estimated frequency for the pressure fluctuation as $f \sim c/(4L) \approx 2.69$ kHz. In the analysis, the surface vibration is very much reduced due to the gluing of the sensor on the top of the tube. To detect this small amplitude, we sliced the video as a function of time (fig. SI-6(a)), then binarized and digitized it (fig. SI-6(b)). By performing the Fast Fourier Transformation, we obtained the frequency peak of the surface vibration at 2.99 kHz (fig. SI-6(c)), which fairly agrees with that of the pressure wave. In addition, we also checked the frequency of the acceleration data for this particular case. It showed a peak of 3.09 kHz, which is also in reasonable agreement. From the above, we concluded that the vibration of the free surface is directly related to that of the pressure wave and the acceleration.

In addition, we measured acceleration at the impact while mounting an accelerometer on either the

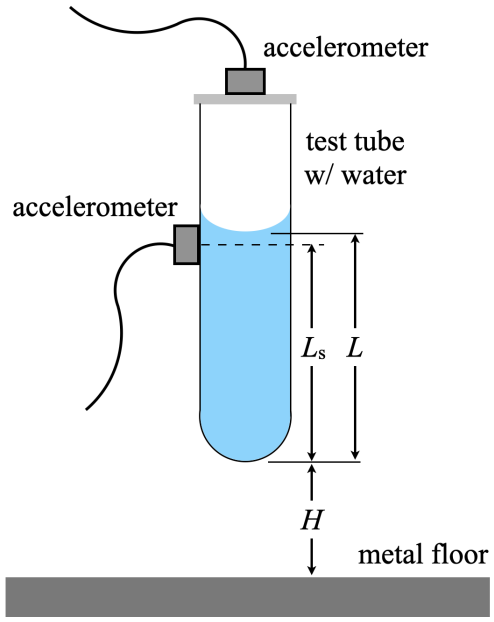

Figure SI-7: Schematic of the experimental setup, where the accelerometer was placed on either the top seal or the side wall of the tube. When it is mounted on the side wall, the accelerometer location is slightly lower than the initial free surface ($L > L_s$).

top of the container (the same as the previous experiments) or the side wall of the tube (see figure SI-7) for more direct discussion. We used purified water, which was filled up to a height of (approximately) 90 mm from the bottom. The outer tube diameter was $d_{out} \approx 16.5$ mm and the thickness of the tube wall was $h \approx 1.1$ mm (i.e., the thinnest wall condition). Note that the accelerometer is designed to measure the force in one direction so we had to switch the sensor location.

First, we compare the frequency response at the impact for each direction (see figure SI-8). The drop height of the tube was set to $H \approx 3$ mm to reduce a chance of the cavitation onset. We used the same plastic glue as before to mount the sensor. By repeating the measurement 3 times for each condition, we found some general trends. (1) the amplitude of the vibration (i.e., acceleration data) measured at the top (see blue lines) tends to be significantly larger than that when measured at the side (see red lines), and (2) there were different frequency responses, where the primary peak is found at ~ 4 kHz when measured on the top and ~ 7 kHz when measured at the side as marked by vertical dashed lines.

A significant difference in the amplitude implies that, in this impact event, the vertical component is more dominant than the radial one. This trend was also confirmed in other sets of experiments (see figure SI-9(a)), where we dropped a tube from $H \approx 50$ mm while testing two different glues to ensure it did not affect the qualitative result. In this figure, plastic glue represents what we have used for other previous tests, while hot glue means a slightly softer one we used for comparison. In such cases, as the tube drop height is sufficiently large, cavitation may occur and thus the frequency response could not be reliably computed. However, it was clear that the accelerometer on the top of the container recorded a larger peak (see figure SI-9(a)), supporting our results in figure SI-8.

In terms of the frequency response in figure SI-8, the primary peak found from the accelerometer on the top was about 4.16 kHz. Our simple estimation for the pressure wave propagation in the water column (in the vertical direction) was estimated to be $f \sim c/(4L) \approx 1483/0.36 \approx 4.12$ kHz, which was

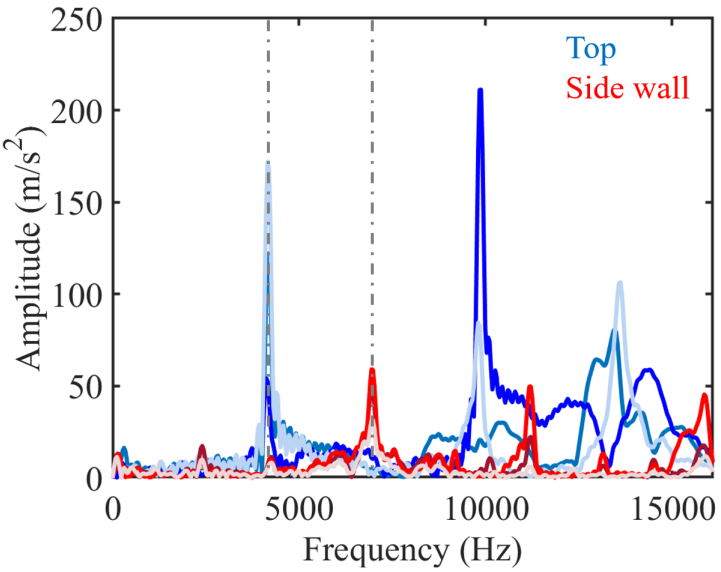

Figure SI-8: Comparison of frequency responses measured at either top (blue) or side wall (red) of the tube. Vertical dashed lines shows frequency peaks found in each measurement series. The tube was dropped from $H = 3$ mm above a metal floor.

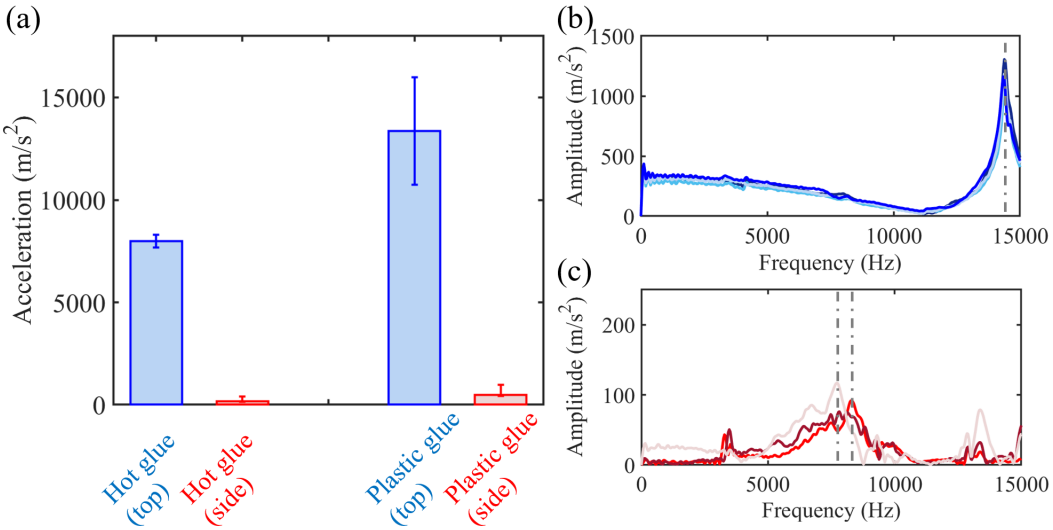

Figure SI-9: (a) Comparison of the acceleration peaks due to the initial impact measured at the top (blue) and at the side (red), for plastic glue and hot glue. The tubes were dropped from $H = 50$ mm. (b) Frequency response of empty tube measured at the top of the container dropped from $H = 15$ mm. Five individual runs are presented. (c) Frequency response of empty tube measured at the side wall of the tube dropped from $H = 50$ mm. Vertical dashed lines show the upper and lower bounds for three trials.

reported to be similar to the fluid interface's vibration frequency as discussed above. A fair agreement between the two suggests that vertical wave propagation governs the acceleration as well as the interface vibration, which is consistent with the discussion above. We note that there are noticeable frequency peaks at higher frequencies when we measured it at the top of the tube (figure SI-8, at $f \gtrsim 1.0 \times 10^4$ Hz). These frequency peaks are not very reproducible, and we speculate they might be related to the cavitation onset, while we attempted to reduce it. Other possible factors include the mechanical vibration of the sensor and systems, or the tube resonance (see figure SI-9(b)), among others.

We note that, when we placed the sensor on the wall of the tube, we found a peak at around 6.98 kHz, which we are not aware of its origin. While the theoretical answer for this is yet unknown, meanwhile, we dropped an empty container from $H \approx 40-50$ mm, in which we found a peak at a similar range (7.71 - 8.28 kHz, see figure SI-9(c)). This might suggest that the peak frequency for the side measurement in figure SI-8 is not related to the fluid mass displacement but to the resonance of the container itself. It does not mean that the container's (radial) vibration/deformation is irrelevant to the fluid interface vibration. However, at the same time, perhaps we can say that vertical wave propagation plays one of the key roles in determining the motion of the container and thus the interface vibration, as we argued in the manuscript.

3 Cavitation in a hydrogel system

The onset of cavitation and the associated dynamics are of great interest in the community, as they contribute to understanding the brain injuries that may occur following a sudden impact (Barney *et al.*, 2020; Marsh & Bentil, 2021). Though a similar system observed the onset of cavitation in a gelatin hydrogel using a high-speed camera (Pan *et al.*, 2017), the present study did not perform any direct visualizations. However, comparing acceleration data as a function of time, some cases exhibit enhanced signals at $O(1)$ ms after the impact (see figure SI-10). These might be related to the perturbation inside the gelatin column, namely the onset of cavitation. This result supports our claim that the present research has the potential to clarify our understanding of acceleration-induced brain injuries, although the sensitivity of measurements is limited.

References

BARNEY, C. W., DOUGAN, C. E., MCLEOD, K. R., KAZEMI-MORIDANI, A., ZHENG, Y., YE, Z., TIWARI, S., SACLIGIL, I., RIGGLEMAN, R. A., CAI, S., LEE, J. H., PEYTON, S. R., TEW, G. N. & CROSBY, A. J. 2020 Cavitation in soft matter. *Proc. Natl. Acad. Sci.* **117** (17), 9157–9165.

KIYAMA, A., TAGAWA, Y., ANDO, K. & KAMEDA, M. 2016 Effects of water hammer and cavitation on jet formation in a test tube. *J. Fluid Mech.* **787**, 224–236.

MARSH, J. L. & BENTIL, S. A. 2021 Cerebrospinal fluid cavitation as a mechanism of blast-induced traumatic brain injury: A review of current debates, methods, and findings. *Front. Neurol.* **12**, 626393.

PAN, Z., KIYAMA, A., TAGAWA, Y., DAILY, J., THOMSON, S., HURD, R. & TRUSCOTT, T. T. 2017 Cavitation onset caused by acceleration. *Proc. Natl. Acad Sci.* **114** (32), 8470–8474.

TERWAGNE, DENIS & BUSH, JOHN W M 2011 Tibetan singing bowls. *Nonlinearity* **24** (8), R51.

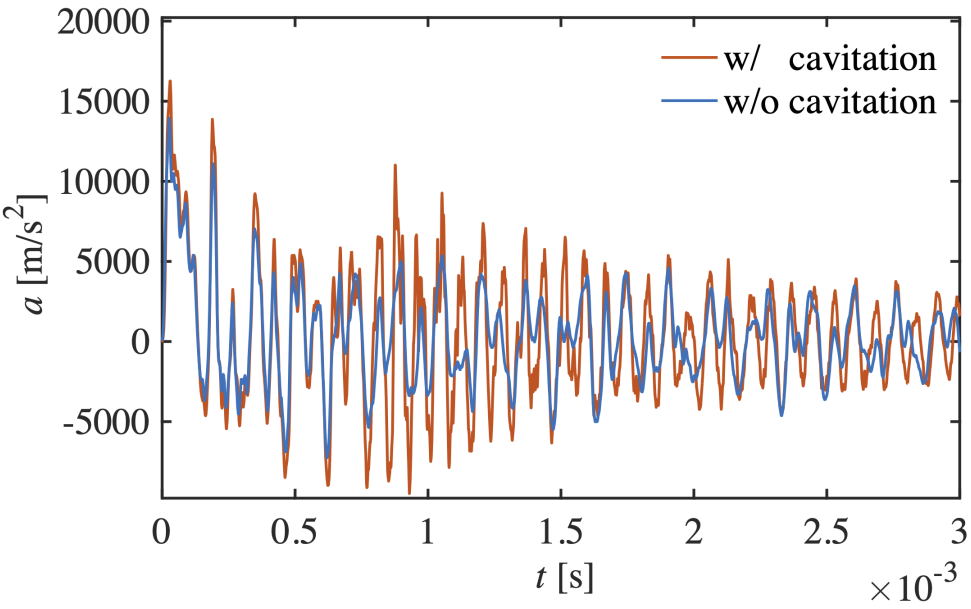

Figure SI-10: Acceleration a (m/s^2) measured as a function of time t (s). The orange line represents the data with cavitation, while the blue line shows data without cavitation onset. The liquid column height and drop height are $L = 60$ mm and $H = 15$ mm. The Strouhal number St is expected to be greater than 0.2. The signals have not been low-pass filtered to avoid the elimination of high-frequency responses caused by bubble activity.

YUKISADA, R., KIYAMA, A., ZHANG, X. & TAGAWA, Y. 2018 Enhancement of focused liquid jets by surface bubbles. *Langmuir* **34** (14), 4234–4240.